Phase-Field Simulation of a Dynamic Protective Layer for the Inhibition of Dendrite Growth in Zinc Metal Batteries.

Bharat Pant¹, Yao Ren¹, Ye Cao^{1,*}

¹Department of Materials Science and Engineering, University of Texas at Arlington, Arlington, Texas, 76019 USA

Corresponding author: Ye Cao

*Email: <u>ye.cao@uta.edu</u>

Phone: +1 (817) 272-1858

Address: ELB 332, 501 W 1st St., Arlington, TX, 76019 USA

ABSTRACT

Metallic zinc (Zn) has been considered one of the most promising anode materials for nextgeneration aqueous Zn batteries due to its low redox potential and high storage capacity. However, excessive dendrite formation in Zn metal, corrosion, the evolution of hydrogen gas during the cycling process, and the poor Zn-ions (Zn²⁺) transport from the electrolyte to the electrode limits its practical application. One of the most effective strategies to suppress Zn dendrite growth and promote Zn²⁺ transport is to introduce suitable protective layers between the Zn metal electrode and the electrolyte. Herein, we mathematically simulated the dynamic interactions between the Zn deposition on the anode and the resulting displacement of a protective layer that covers the anode, the latter of which can simultaneously inhibit Zn dendrite growth and enhance the Zn²⁺ transport through the interface between Zn anode and the protective layer. Our simulation results indicate that a protective layer of high Zn²⁺ diffusivity not only improves the deposition rate of the Zn metal but also prevents the dendrite growth by homogenizing the Zn²⁺ concentration at the anode surface. In addition, it is revealed that the anisotropic Zn²⁺ diffusivity in the protective layer influences the 2D diffusion of Zn²⁺. Higher Zn²⁺ diffusivity perpendicular to the Zn metal surface inhibits the dendrite growth, while higher diffusivity parallel to the Zn metal surface promotes dendrite growth. Our work thus provides a fundamental understanding and a design principle of controlling anisotropic Zn²⁺ diffusion in the protective layer for better suppression of dendrite growth in Zn metal batteries.

Keywords: phase-field simulation, zinc metal battery, dendrites growth, anisotropic diffusion, protective layer

1. Introduction

The current market of power supply for portable electronic devices and electric vehicles is dominated by Lithium-ion batteries (LIBs) due to their high energy density and long lifetime. ^{1,2} However, traditional LIBs using graphite as anode materials have reached their theoretical limits and hence cannot meet the growing demand for energy storage. ³ One potential solution is to replace graphite with lithium (Li) metal for anode materials. However, the use of toxic organic electrolytes, the scarcity of Li metal resources, and the severe Li dendrite growth issues prevent its practical application. 1,4 Recently, zinc metal battery (ZMB) has been considered one of the most promising next-generation batteries because of the use of non-toxic aqueous electrolyte, abundance of Zn metal on the earth, low redox potential (-0.762 V versus standard hydrogen electrode), and high theoretical capacity (820 mAh/g). 5,6 However, ZMB also suffers from uncontrollable Zn dendrite growth that hinders its practical applications. During cycling the Zn anode deposits irregularly, resulting in spiky structures known as dendrites. ⁷ These dendrites not only decrease the capacity of the battery but can also penetrate the separator and reach the cathode side, resulting in an internal short circuit that leads to failure of the battery and other safety issues. ⁸ Additionally, in aqueous electrolytes, Zn is thermodynamically active and the direct contact between Zn metal and the mild aqueous electrolyte could result in the dissolution of Zn, the hydrogen evolution reaction (HER), and the formation of by-products such as Zn₄(OH)₆SO₄.xH₂O. 9,10 The continuous production of hydrogen gas causes electrolyte leakage and the swelling of a sealed battery due to an increase in internal pressure. 11

Over the years, several strategies have been developed to suppress the Zn dendrite growth and to improve the performance of Zn metal batteries, such as creating an artificial solid-electrolyte interface (SEI) layer, ^{6,12-14} adding additives in the electrolyte solution to regulate the electrodeposition kinetics, ¹⁵⁻¹⁷ replacing liquid electrolyte with solid polymer electrolytes, ¹⁸⁻²⁰

and coating a protective layer on Zn metal surface that can physically prevent the Zn dendrite growth. ^{4,7,21} It has been reported that rampant 2D diffusion of Zn²⁺ could be the reason for Zn dendrite growth in Zn metal batteries. ²² Hence, an effective strategy to inhibit Zn dendrite growth is to promote Zn²⁺ to move in the horizontal direction (perpendicular to the anode surface) and inhibit its lateral movement (parallel to the anode surface). ²³ Therefore, the ideal protective layer should have higher Zn²⁺ ionic conductivity to restrain 2D diffusion, low electron transference number, and good mechanical strength. ^{24,25} The higher ionic conductivity facilitates the diffusion of Zn²⁺ through the electrolyte/electrode interface and hence prevents Zn²⁺ concentration polarization, whereas the high mechanical strength prevents the dendrites from physically damaging the protective layer. ²⁶ For instance, Zhang et al. ²¹ synthesized Zn-Sb₃P₂O₁₄ as an artificial protective layer filled with novel 2D Zn²⁺ adsorbed Sb₃P₂O₁₄³⁻ nanosheets to mitigate the dendrite growth in the Zn metal battery. The protective layer builds the channels that allow Zn to deposit only along the horizontal direction and block 2D diffusion, enabling dendrite-free Zn deposition. Recently, Mu et al. 9 developed a ZnF2-Cu (in-situ) protective layer to inhibit dendrite growth and suppress corrosion on Zn metal due to side reactions with electrolytes. The protective layer enables Cu particles, which act as heterogenous seeds, to distribute uniformly along the Zn surface, resulting in the homogenous deposition of Zn. In addition, the ZnF₂-Cu layer acts as a barrier to separate the Zn anode from the electrolyte, preventing the formation of byproducts and corrosion. More recently, researchers have successfully synthesized protective layers to effectively stabilize the Zn battery, such as spirally grown 3D ZnCo overlayer, ²⁷ self-assembled multilayers (SAM) consisting of L-cysteine, ²⁸ and tetramethylene sulphone (TMS) acting as a hydrated deep eutectic electrolyte. ²⁹ On the other hand, some researchers have focused on developing an artificial solid-electrolyte interface (SEI) layer to suppress dendrite growth and avoid corrosion reactions.

For example, Yang *et al.* ²⁴ constructed an artificial SEI layer consisting of Mg-Al layered double hydroxide (LDH). The SEI layer facilitates the Zn²⁺ diffusion from electrolyte to electrode, thus enabling the even distribution of Zn²⁺ and inhibition of dendrite growth. The SEI layer also improves the Coulombic efficiency by preventing hydrogen evolution reactions and H₂O-induced corrosion.

In parallel, computational method such as phase-field modeling has emerged as a powerful tool to simulate dendrite growth in Li, Zn, and Mg-based metal batteries. Based on the earlier phase-field model of electrochemistry, ^{30,31} Liang et al. and Chen et al. developed nonlinear phasefield models to study the electrodeposition kinetics in batteries. 32-34 These models were further extended to investigate multiple factors on the dendrite growth, such as the elastic and plastic strain in the electrode and electrolyte, ³⁵⁻³⁷ the grain size and the grain boundary, ^{38,39} the applied voltage and current, ⁴⁰ the temperature, ^{41,42} and the applied external pressure. ⁴³ However, very few models studied the effect of a protective layer on dendrite formation and growth, due to the difficulties in simulating a dynamic protective layer that evolves with the metal anode deposition. The protective layer should remain attached to the Zn anode surface and move along with it during Zn deposition. Thus, in the simulation the displacement rate of the protective layer (v_n) should be equal to the rate of the Zn anode/electrolyte interface movement during deposition (v_{Zn}) . Otherwise, the protective layer may either delaminate from the Zn electrode when $v_p > v_{Zn}$, or unrealistically block the normal Zn electrode deposition when $v_p < v_{Zn}$, neither of which is realistic from experimental observations. In addition, very few studies have been conducted to investigate the effect of the anisotropic diffusivity of the Zn2+ in the protective layer, although it could significantly affect the Zn deposition rate and dendrite morphology.

In this study, we developed a phase-field model to simulate the dynamic interactions between the Zn metal deposition and the protective layer displacement in Zn metal batteries. Our simulation results indicate that the protective layer remains on top of the Zn metal, physically blocks the dendrite growth, and enhances the transport of Zn²⁺. The protective layer reduces the high local electric field and large concentration gradient at the Zn surface, enabling the smooth deposition of Zn metal. In addition, it is found that ion diffusion behavior in the protective layer plays an important role in the suppression or promotion of the dendrites. Our simulation thus provides new insight into the roles of isotropic and anisotropic Zn²⁺ diffusion in the growth and morphology of dendrites in Zn metal batteries.

2. Methods

In this work, we consider a half-cell model consisting of a Zn metal anode, a protective layer that covers the anode, and an electrolyte solution. To differentiate these different regions, we employ two order parameters, ξ_1 and ξ_2 to represent the Zn metal anode ($\xi_1 = 1, \xi_2 = 0$), the protective layer ($\xi_1 = 0, \xi_2 = 1$), and the electrolyte solution ($\xi_1 = 0, \xi_2 = 0$), respectively. The values of ξ_1 and ξ_2 continuously change from 0 to 1 across the Zn electrode/protective-layer interface and protective-layer/electrolyte interface. The electrolyte solution consists of positive Zn²⁺ and effective negative ions (A²⁻), the latter of which is the combination of all the remaining cations and anions. Only Zn²⁺ is assumed to be mobile. Additionally, we assume that Zn metal can always provide sufficient electrons (e⁻) at its surface to reduce the arriving Zn²⁺ into Zn atom (Zn²⁺ + 2e⁻ = Zn) and deposit on the Zn metal surface. Finally, the protective layer is assumed to be ionically conductive (for Zn²⁺) and electrically insulating. For simplicity, we do not consider the

temperature effect in our current model, and the entire system is assumed to be isothermal. The half-cell model is illustrated in **Figure 1**.

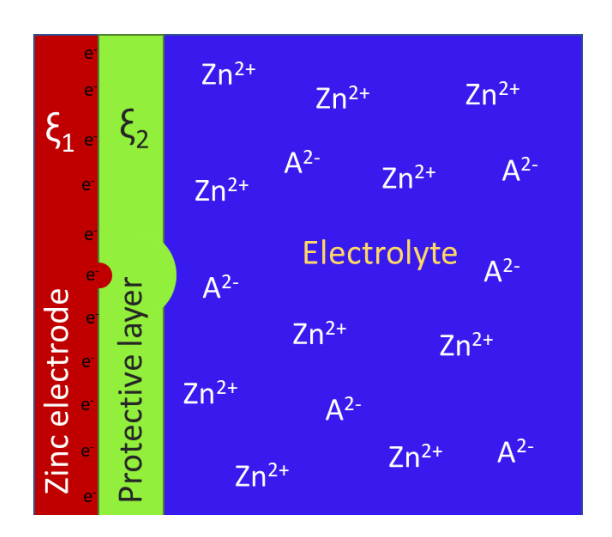


Figure 1. Schematic illustration of a half-cell battery consisting of a Zn metal electrode, a protective layer, and an electrolyte solution. The electrolyte solution contains cations (Zn^{2+}) and effective anions (A^{2-}) .

The total free energy of the system is given by the following equation,

$$F = \int_{V} [f_{ch}(\xi_1, \xi_2, C_i) + f_{grad}(\nabla \xi_1, \nabla \xi_2) + f_{elec}(C_i, \phi)] dV \qquad (1)$$

where f_{ch} is the Helmholtz free energy density, f_{grad} is the gradient energy density, and f_{elec} is the electrostatic energy density. The Helmholtz free energy consists of energy of ion mixing (f_{lon}) and local free energy density (f_0) . The energy of mixing is given by $f_{lon} = C_0RT\sum_i C_i^* lnC_i^*$, where C_i^* is a dimensionless concentration $(C_i^* = C_i/C_0)$, and the local free energy density is given by $f_0 = g(\xi_1, \xi_2) = W_1\xi_1^2(1-\xi_1)^2 + W_2\xi_2^2(1-\xi_2)^2 + \frac{A}{2}\xi_1^2\xi_2^2$, where W_1 and W_2 are the energy barrier heights of double-well functions for order parameters ξ_1 and ξ_2 , respectively, and $\frac{A}{2}\xi_1^2\xi_2^2$ is a cross-term that yields three equilibrium states: for the electrode $(\xi_1 = 1, \xi_2 = 0)$, for the protective layer $(\xi_1 = 0, \xi_2 = 1)$, and for the electrolyte $(\xi_1 = 0, \xi_2 = 0)$. The values of W_1 and

 W_2 are selected to be 0.25 and 0.15, respectively, and the value of the coefficient $\frac{A}{2}$ is chosen to be 1.5. The gradient energy density takes the form $f_{grad} = \frac{\kappa_1}{2} (\nabla \xi_1)^2 + \frac{\kappa_2}{2} (\nabla \xi_2)^2$, where κ_1 and κ_2 are gradient energy coefficients of Zn metal and protective layer, respectively. To simulate the dendritic morphology of Zn metal, the anisotropic gradient energy coefficient for the Zn anode is introduced, which is given by $\kappa_1 = \kappa_0 [1 + \delta \cos(\omega \theta)]$, where δ is the strength of anisotropy; ω is the mode of anisotropy; κ_0 is a coefficient related to the Zn metal surface energy, and θ is the angle between the normal vector to the interface and reference axis. Since Zn has a hexagonal close-packed crystal structure, the mode of anisotropy (ω) is set to be 6. ⁴⁴ Finally, the electrostatic energy density is given by $f_{elec}(c_i, \phi) = F \sum_i z_i c_i \phi$, where F is the Faraday constant, z_i is the valence of charge species, and ϕ is the electric potential. More details about the derivations of these energy densities can be found in the literature. ³⁴

The growth rate of the Zn metal anode due to Zn^{2+} deposition is described by the temporal evolution of ξ_1 and governed by the following equation,

$$\frac{\partial \xi_1}{\partial t} = -L_{\xi_1} \left\{ \frac{\partial f_{ch}}{\partial \xi_1} - \kappa_1(\nabla^2 \xi_1) \right\} - L_{\eta} h'(\xi_1) \left\{ exp \left[\frac{\alpha z F \eta}{RT} \right] - C_{Zn^{2+}} exp \left[-\frac{\beta z F \eta}{RT} \right] \right\}$$
(2)

where L_{ξ_1} is the interfacial mobility, L_{η} is the electrodeposition reaction constant, and t is the time. $h'(\xi_1)$ is the first derivative of an interpolation function $h(\xi_1) = {\xi_1}^3 (6{\xi_1}^2 - 15{\xi_1} + 10)$, which confines the Butler-Volmer driving force that arises from the charge transfer reaction $(Zn^{2+} + 2e^- = Zn)$ to be at the Zn/protective layer interface. α and β are the symmetric factors $(\alpha + \beta = 1)$, R is the universal gas constant, T is the absolute temperature, z is the charge number $(z = 2 \text{ for } Zn^{2+})$, and η is the overpotential.

The displacement of the protective layer induced by Zn metal surface movement is described by the evolution of the order parameter ξ_2 ,

$$\frac{\partial \xi_2}{\partial t} = -L_{\xi_2} \left\{ \frac{\partial f_{ch}}{\partial \xi_2} - \kappa_2(\nabla^2 \xi_2) \right\} - D_f \tag{3}$$

where L_{ξ_2} is the interfacial mobility of the protective layer, κ_2 is the gradient energy coefficient, D_f is the driving force term for the protective layer displacement due to the Zn metal surface movement during deposition. Based on the relationship between diffuse interface velocity and effective driving force, we defined D_f as, ⁴⁵

$$D_f = \max[-h'(\xi_1) \times h'(\xi_2) \times \Delta G] \times b \times \frac{\partial \xi_2}{\partial x}$$
 (4)

where $\Delta G = \left\{exp\left[\frac{azF\eta}{RT}\right] - C_{Zn^{2+}} exp\left[-\frac{\beta zF\eta}{RT}\right]\right\}$ is the Butler-Volmer expression taken from Equation (2), and the driving force constant b is selected to guarantee that no interfacial delamination between Zn metal and the protective layer would occur (the value of "b" can be found in Table 1). The 'max' function takes the maximum value of the product $h'(\xi_1) \times h'(\xi_2) \times \Delta G$, where $h'(\xi_1) \times \Delta G$ is the driving force acting at the surface of the order parameter ξ_1 , so that the same force would be applied on both surfaces of ξ_2 . Additionally, the product $h'(\xi_1) \times h'(\xi_2)$ ensures that driving force becomes zero if Zn metal and the protective layer are not in contact with each other, where $h'(\xi_2)$ is the first derivative of the interpolation function $h(\xi_2) = \xi_2^{-3}(6\xi_2^{-2} - 15\xi_2 + 10)$. The details on the derivation of the driving force can be found in the supporting information.

The evolution of Zn²⁺ concentration in both the electrolyte and the protective layer is governed by the Nernst-Planck equation,

$$\frac{\partial c_{Zn^{2+}}}{\partial t} = \nabla \cdot \left[D^{eff} \nabla C_{Zn^{2+}} + \mu_{Zn} C_{Zn^{2+}} z F \nabla \phi \right] - K \frac{\partial \xi_1}{\partial t}$$
 (5)

where D^{eff} is the effective diffusivity of Zn^{2+} , which is expressed by using the interpolation functions $h(\xi_1)$ and $h(\xi_2)$, i.e., $D^{eff} = D_e h(\xi_1) + D_p h(\xi_2) + D_s (1 - h(\xi_1) - h(\xi_2))$, where, D_e , D_p , and D_s are the diffusivity of Zn^{2+} in the Zn electrode, the protective layer, and the electrolyte, respectively. μ_{Zn} is the mobility of Zn^{2+} , K is the accumulation constant, and ϕ is the electric potential. $K \frac{\partial \xi_1}{\partial t}$ in Equation (5) is a source term to describe the annihilation/accumulation rate of the Zn^{2+} caused by the charge transfer reaction ($Zn^{2+} + 2e^- = Zn$) at the anode surface.

The system is assumed to be charge neutral and the current density is conserved. The electric potential distribution is calculated by solving the current continuity equation which is written as,

$$\nabla \cdot (\sigma^{eff} \nabla \phi) = R_e \frac{\partial \xi_1}{\partial t} \tag{6}$$

where R_e is the current constant, σ^{eff} is the effective electrical conductivity whose value is calculated using the interpolation function as $\sigma^{eff} = \sigma^e h(\xi_1) + \sigma^p h(\xi_2) + \sigma^s (1 - h(\xi_1) - h(\xi_2))$, where σ^e , σ^p and σ^s represent the electrical conductivities of the electrode, the protective layer, and the electrolyte, respectively. For simplicity, we assume that $\sigma^p = \sigma^s$ in our simulations.

All the simulations were performed on the COMSOL Multiphysics software using a phase-field approach. Equations (2), (3), (5), and (6) are solved by finite element methods using general PDE and a time-dependent solver. The system size is chosen to be $500 \times 500 \, \mu \text{m}^2$. The mesh size is applied manually, and the maximum element size is set to be 2.75 μ m. The real values of all the parameters are converted into normalized values. The real values are normalized in terms of characteristics energy E_0 , the characteristics time Δt_0 , and the characteristics length l_0 . The real values and the normalized values are listed in Table 1. Dirichlet boundary conditions are applied to solve the Zn^{2+} concentration ($C_{Zn^{2+}}$) and electric potential (ϕ), while zero flux boundary conditions are applied for order parameters ξ_1 and ξ_2 . The value of ϕ is set to be -0.18 V at the

anode (left boundary) and 0 V at the right boundary of the half-cell, whereas the value of $C_{Zn^{2+}}$ is set to be 1 at the right boundary (**Figure S1**). The initial value of the Zn^{2+} concentration in the electrolyte solution is assumed to be 1. The value of $C_{Zn^{2+}}$ is normalized by dividing it with the bulk concentration of Zn^{2+} ions, i.e, $C_{Zn^{2+}} = C_{Zn}/C_0$, where $C_0 = 1 \, mol/L$. The simulation is performed at room temperature (T = 298 K).

Table 1: Parameters and their normalized values.

Parameters	Sym bol	Real Value	Normalization	Normalized value	Reference
Interfacial mobility 1	L_{ξ_1}	$1.33 \times 10^{-6} m^3 / (I \times s)$	$\hat{L}_{\xi 1} = L_{\xi 1} \times (E_0 \times \Delta t_0)$	3330	Estimated
Interfacial mobility 2	$L_{\xi 2}$	$2.65 \times 10^{-7} m^3 / $	$\hat{L}_{\xi 2} = L_{\xi 2} \times (E_0 \times \Delta t_0)$	665	Estimated
Reaction constant	L_{η}	0.001/s	$\hat{L}_{\eta} = L_{\eta} \times \Delta t_{0}$	1	35
Ion diffusivity in Electrolyte	D_s	$1\times 10^{-11}m^2/s$	$\widehat{D}_s = D_s / (l_0^2 / \Delta t_0)$	1	Estimated
Ion diffusivity in Electrode	D_e	$1\times 10^{-14}~m^2/s$	$\widehat{D}_e = D_e / (l_0^2 / \Delta t_0)$	0.001	Estimated
Electrical conductivity of electrolyte	$\sigma_{\scriptscriptstyle S}$	0.1 <i>S/m</i>	$\hat{\sigma}_s = \frac{\sigma_s / ((l_0^2 / \Delta t_0) \times (c_0 F^2 / RT))}$	2	44
Electrical conductivity of electrode	σ_e	$1 \times 10^7 S/m$	$\hat{\sigma}_e = \frac{\sigma_e}{((l_0^2 / \Delta t_0) \times (c_0 F^2 / RT))}$	2 × 10 ⁸	35
Gradient energy coefficients	k_{1}, k_{2}	$5\times 10^{-5}J/m$	$\hat{k} = k/(E_0 \times l_0^2)$	0.002	34
Surface energy	Υ	$0.5 \ J/m^2$	$\widehat{Y} = Y/(E_0 \times l_0)$	0.002	46
Charge transfer coefficient	β , α	0.5	-	-	46
Driving force constant	b	$6\times10^{-10}\ m/s$	$\hat{b} = b \times (\Delta t_0/l_0)$	0.006	Calculated

3. Results and discussions

3.1. Dendrite growth in a bare Zn anode.

First, we investigate the evolution of the Zn anode in the absence of a protective layer. The initial morphology (t = 0 s) of the Zn anode has a flat surface, and a small semi-circle-shaped protrude is introduced at the surface center to mimic the surface roughness, as shown in **Figure**

2(a). The protrude acts as a nucleation site for Zn dendrite growth. The initial Zn²⁺ concentration and electric potential distribution (t = 0 s) are shown in Figure 2 (d) and (g) and will be the same for all our simulations hereafter. Equations (2), (5), and (6) are solved self-consistently to obtain the evolutions of the Zn anode (ξ_1) , Zn^{2+} concentration $(\mathcal{C}_{Zn^{2+}})$, and electrical potential (ϕ) distribution, as shown in Figure 2. It is seen that in the absence of a protective layer, the initial bare Zn metal anode grows from a protrude into filament-like large dendritic structures (Figure 2 (b), (c)), due to the large concentration gradient of Zn²⁺ (Figure 2 (e), (f)) and large electric field intensity at the tip of the protrude (Figure 2 (k) inset). This can be clearly seen by the 1-D plots of Zn^{2+} concentration and electric field along the x direction (E_x) across the tips of Zn dendrite at t = 300 s (red curves in Figure 2(j) and (k)). These large gradients act as a driving force for Zn metal to grow preferentially across the dendrite tips. ⁴⁷ By contrast, the Zn metal plain surface grows dendrite-free at the top and bottom regions, where only small dendrites can be seen as a result of the presence of small surface roughness. This can be further explained by the 1-D plot of Zn²⁺ concentration across the plain Zn metal surface which shows a smooth concentration gradient (black curve in Figure 2(j)). Finally, the local electric field is segregated at the tip of the dendrites (inset of Figure 2(k)). Its maximum value reaches \sim -0.12 V/ μ m, almost 8 times larger than that at the plain interface (\sim -0.015 V/ μm).

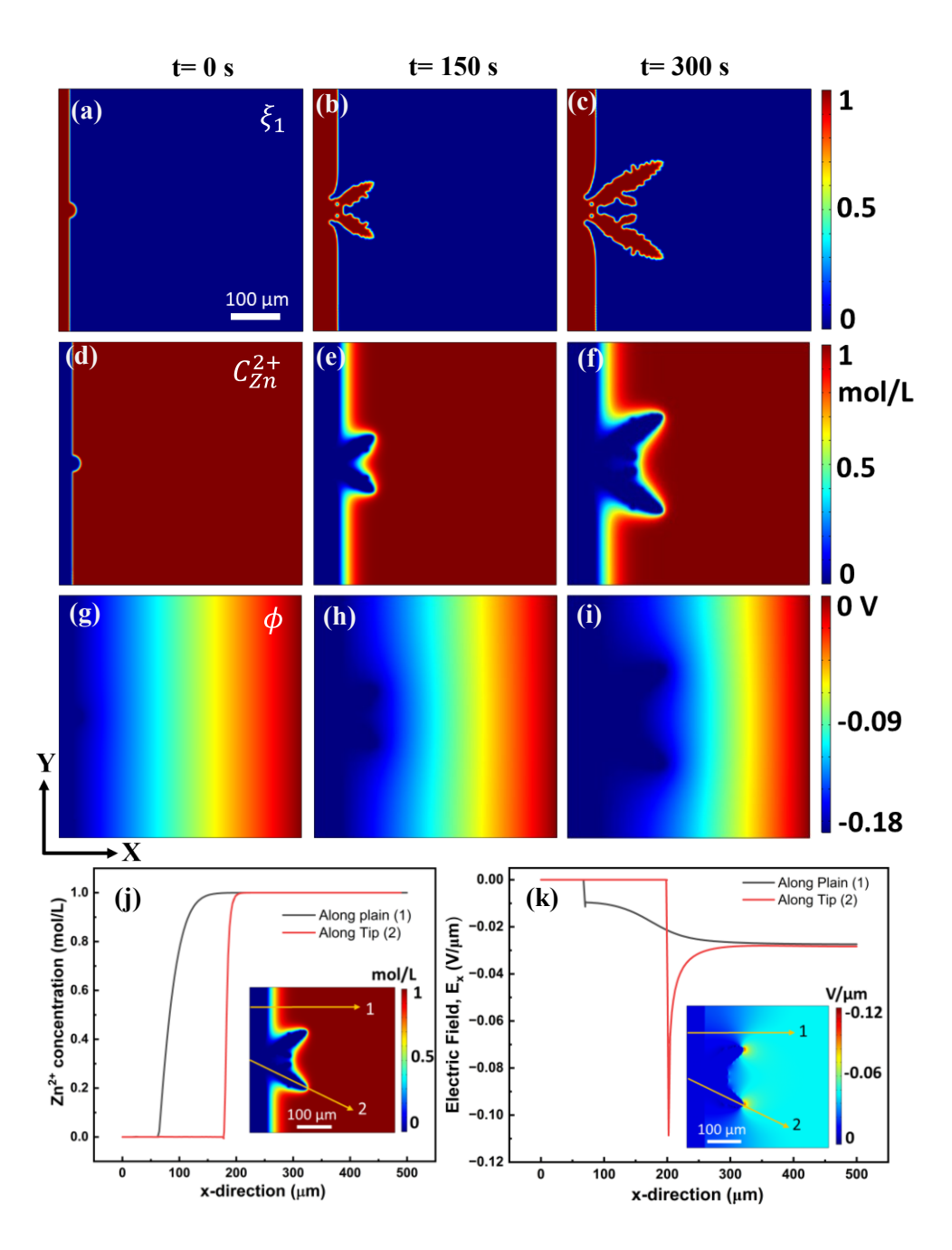


Figure 2. Simulation results for dendrite growth in bare Zn anode. (**a-c**) Zn anode morphology from 0 - 300 s. (**d-f**) Zn²⁺ concentration. (**g-i**) electrical potential distribution. (**j**) 1-D graph of Zn²⁺ concentration along dendrite tip and plain surface, as shown by arrows in the inset image. The inset image is a 2-D plot of Zn²⁺ concentration at t = 300 s. (**k**) 1-D graph of the electric field along the dendrite tip and plain surface, as shown by arrows in the inset image. The inset image is a 2-D plot of the electric field distribution at t = 300 s. The scale bar in (**a**) applies to all the figures (**a-i**).

3.2. Zn deposition in the presence of the protective layer.

Next, we introduced a protective layer to study its effect on Zn metal deposition by selfconsistently solving the coupled Equations (2), (3), (5), and (6). The initial conditions are the same as in Section 3.1, the thickness of the protective layer is assumed to be 50 μm, and the Zn²⁺ diffusivity (D_p) and electrical conductivity (σ_p) in the protective layer are assumed to be the same as those in the electrolyte (D_s, σ_s) . Figure 3(a)~(c) illustrate the temporal evolutions of the Zn metal anode (red region) and the protective layer (green region). Compared with those in **Figure** 2(a)~(c), the initial protrude on the Zn surface maintains its shape and only increases in size during deposition, rather than growing into a filament-like dendrite structure (Figure 2). The flat surface regions of Zn metal grow homogeneously and become thicker. This results in a much smoother Zn metal surface with an almost uniform growth rate (Figure 3(c)). Meanwhile, the protective layer always covers the Zn metal and no interfacial delamination is seen. Thus, our model successfully simulates the inhibition effect of the protective layer on the Zn dendrite growth. Figure 3 also illustrates the evolutions of Zn²⁺ concentration ((d)~(f)) and electrical potential distribution ((g)~(i)). It is seen that Zn²⁺ concentration is higher in both the protective layer and electrolyte and reduces to almost zero in the Zn metal, indicating that Zn²⁺ can diffuse in the protective layer and is reduced into Zn metal at the Zn metal/protective layer interface. Figure 3(j), (k) illustrate the 1-D plots of Zn^{2+} concentration and electric field along the x direction (E_x) across the protrude (red curve) and the plain Zn metal surface (black curve) at t = 300 s (2D plot in the inset). Compared with Figure 2(j), (k), the Zn²⁺ concentration gradients are almost the same at different regions of the Zn metal surface, and the difference between local electric fields at the protrude tip ($\sim -0.04 \text{ V/}\mu\text{m}$) and plain surface ($\sim -0.03 \text{ V/}\mu\text{m}$) with a protective layer is much smaller than that in the bare Zn electrode (Figure 2(k)). These results indicate that the protective

layer improves the homogeneity of the Zn^{2+} concentration and electric field at the anode surface during battery charging, resulting in dendrite-free Zn deposition. Experimental studies suggest that reducing the large concentration and potential gradient can prevent dendrite growth in Zn metal batteries. 48,49 Thus, our simulation results agree with the previous experimental results.

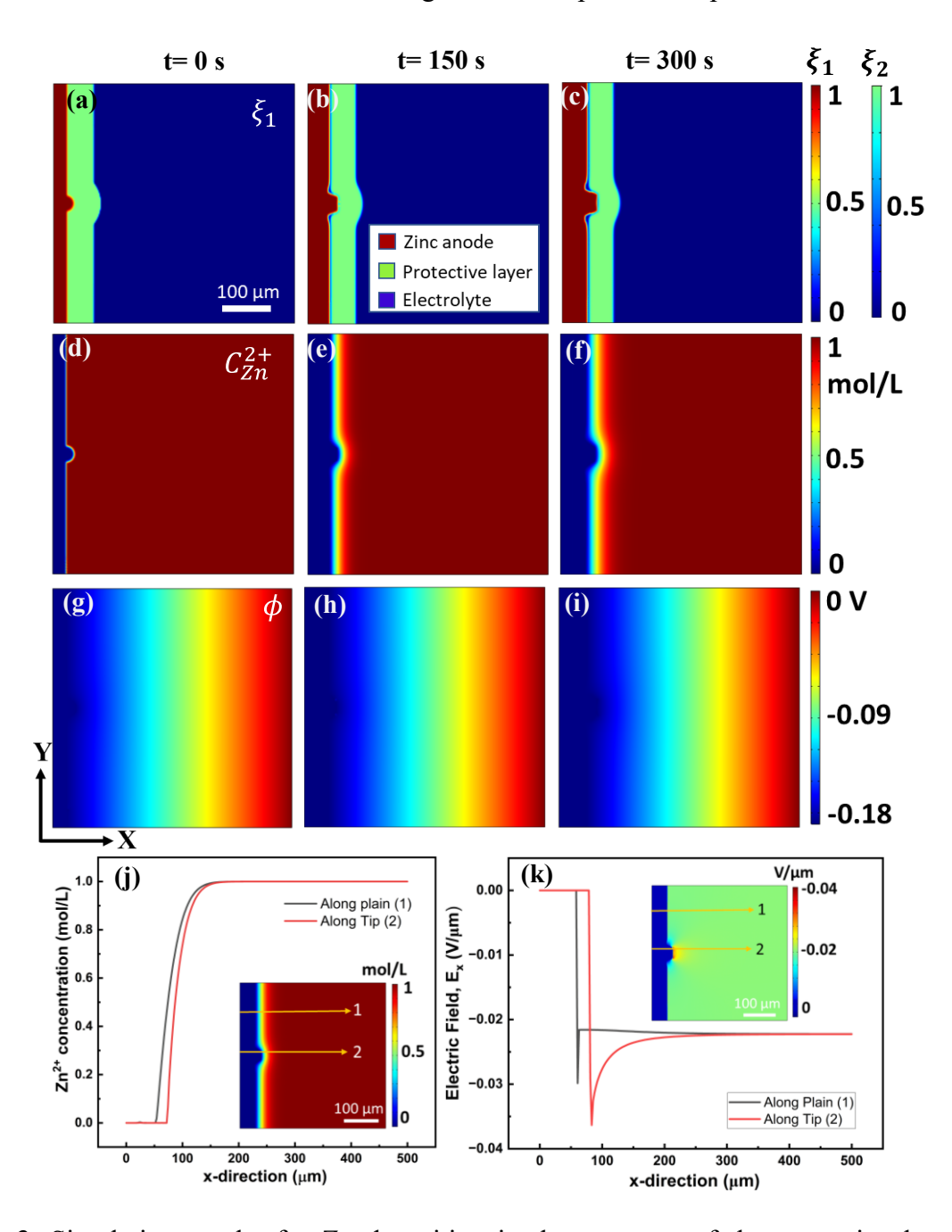


Figure 3. Simulation results for Zn deposition in the presence of the protective layer. (a-c) evolution of Zn metal and protective layer from 0 to 300 s. (d-f) Zn²⁺ concentration. (g-i) electrical

potential distribution. (j) 1-D graph of Zn²⁺ concentration along dendrite tip and flat surface, as shown by arrows in the inset. (k) 1-D graph of the electric field calculated along the arrow's directions, as shown in the inset image. The scale bar in (a) applies to all the figures (a-i).

3.3. Effect of isotropic diffusion of Zn²⁺ in the protective layer on Zn deposition.

It has been previously reported that Zn²⁺ diffusion plays an important role in Zn metal deposition, and constructing a Zn²⁺-affinity protective layer with higher Zn²⁺ transfer kinetics can potentially control the local Zn²⁺ concentration and promote a dendrite-free Zn metal anode.²⁴ The transport of Zn²⁺ in a typical Zn metal battery is dominated by diffusion and drift: the diffusion is induced by the concentration gradient, whereas the drift is induced by the electric potential gradient. ⁵⁰ To further understand its mechanism, we study the effects of Zn²⁺ diffusivity in the protective layer on Zn deposition. We first assume that the protective layer is isotropic and the Zn^{2+} diffusivity along the x direction (perpendicular to Zn metal surface) and y direction (parallel to Zn metal surface) are identical $(D_{px} = D_{py} = D_p)$. Figure 4 illustrate the intermediate (t = 150s) and final morphologies (t = 300 s) of Zn metal and protective layer for four cases: (i) $D_p =$ $0.5D_s$; (ii) $D_p = D_s$; (iii) $D_p = 2D_s$; and (iv) $D_p = 6D_s$. It is clearly seen that when D_p increases, the final thickness of the Zn metal increases accordingly, while the final size of the protrudes is almost the same, as summarized in Figure 5. To understand this behavior, we plot the Zn²⁺ flux (calculated as the product of Zn²⁺ concentration gradient and diffusivity) for these four cases using arrow graphs, as shown in Figure 4(c), (f), (i), and (l). It is seen that when D_p increases, the magnitude of Zn2+ flux (represented by the length of arrows) in the protective layer increases accordingly. The higher Zn²⁺ flux enhances the transport of Zn²⁺, resulting in a higher deposition rate and an increase in the final thickness of Zn metal. It is also seen that in each case, the maximum flux emerges at the Zn metal surface, and the flux direction (represented by the arrow direction) is mostly perpendicular to the Zn metal surface, except in the vicinity of the protrude where the flux is pointing towards the protrude tip. This is because the maximum Zn²⁺ concentration gradient occurs at the Zn metal/protective layer interface and becomes almost zero in both the Zn metal and protective layer. In addition, the Zn²⁺ flux is homogeneous at the Zn surface in each case, indicating that the protective layer facilitates the equal distribution of Zn²⁺ at the surface, which helps reduce the dendrite growth. These results are consistent with prior studies. ^{51,52} Based on our simulation, it can be inferred that the role of the protective layer in Zn metal deposition is two-folded, i.e., it not only blocks the dendrite growth physically but also promotes Zn²⁺ diffusion to realize a larger Zn metal growth rate. The electric field and Zn²⁺ concentration for all these cases are shown in **Figure S2**.

Additionally, we studied the effect of the thickness of a protective layer on Zn deposition. Our simulation results (**Figure S4**) show that when $D_p > D_s$, increasing the thickness of the protective layer will enhance the Zn deposition rate. This is because a highly diffusive protective layer will further facilitate the transport of Zn^{2+} when its thickness increases. In contrast, when $D_p < D_s$, the Zn deposition rate decreases when the thickness of the protective layer increases, as a thicker and less diffusive protective layer will hinder the transport of Zn^{2+} (**Figure S4**).

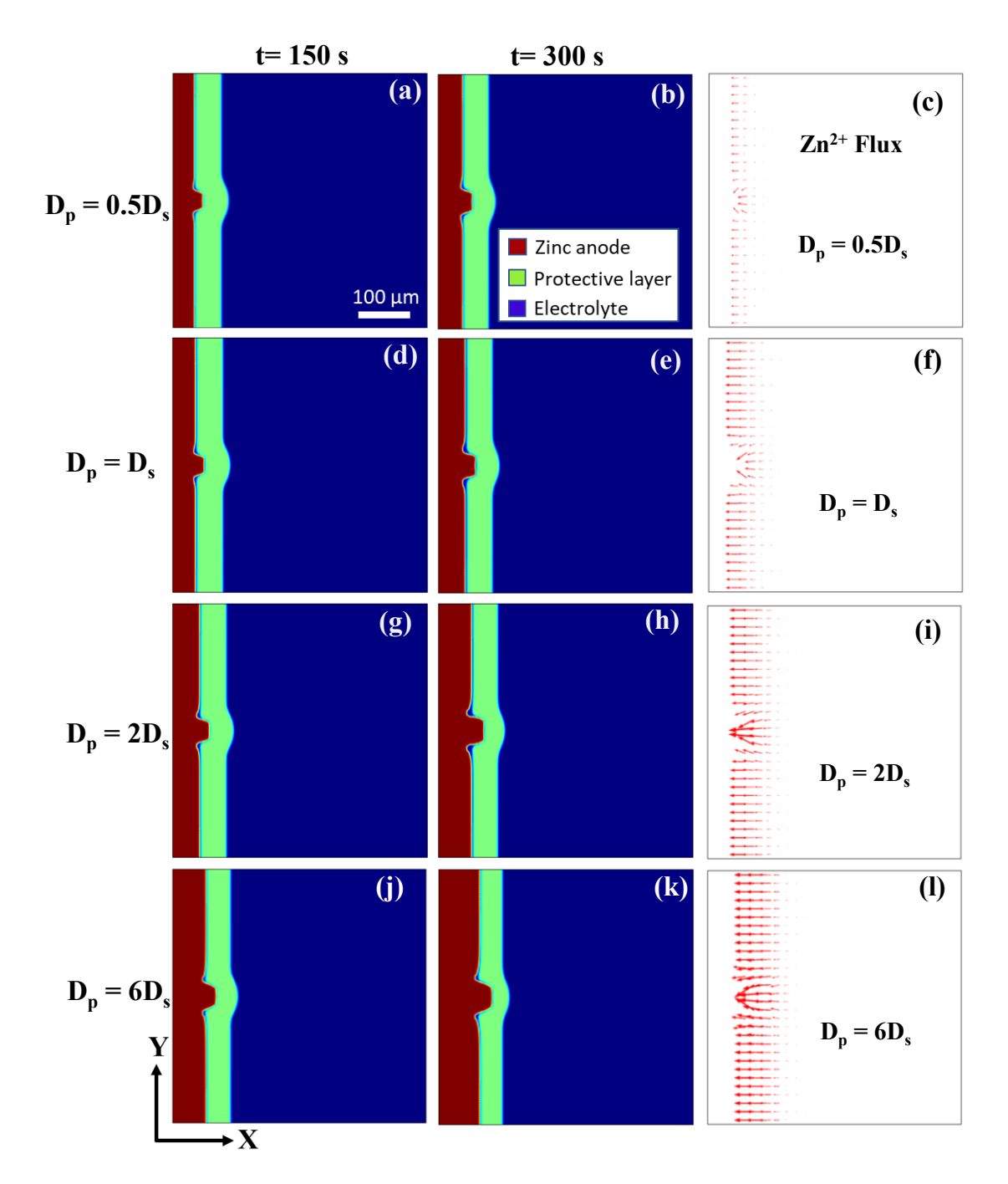


Figure 4. Simulation results showing the morphologies of Zn anode and protective layer at t = 150 s and 300 s with different magnitudes of isotropic diffusivity of Zn^{2+} in the protective layer. (a), (b) when $D_p = 0.5D_s$; (d), (e) when $D_p = D_s$; (g), (h) when $D_p = 2D_s$; (j), (k) $D_p = 6D_s$. (c), (f), (i), (l) arrow graphs showing the magnitudes and directions of the Zn^{2+} flux for four different cases. The scale bar in (a) applies to all the figures (a-l). (D_p and D_s denote the diffusivity of Zn^{2+} in the protective layer and the electrolyte, respectively)

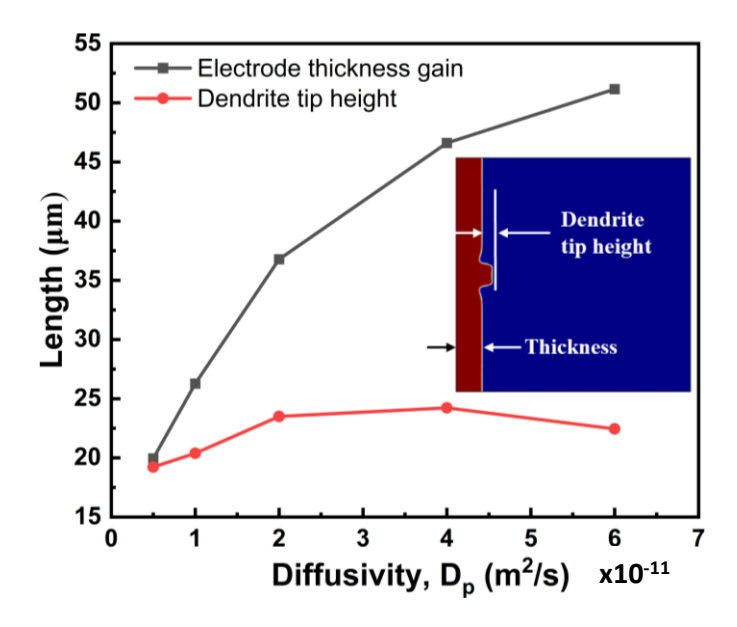


Figure 5. Relationship between diffusivity of Zn^{2+} in the protective layer (D_p) and electrode thickness gain and dendrite tip height. The image in the inset shows how the Zn thickness and tip height are measured. Electrode thickness gain is calculated as the difference between initial thickness (t = 0 s) and final thickness (t = 300 s).

3.4. Effect of anisotropic diffusion of Zn²⁺ in the protective layer on Zn deposition.

Finally, we studied the effect of an anisotropic protective layer in terms of the diffusivity of Zn^{2+} . For an anisotropic protective layer, the diffusivity of Zn^{2+} in the x and y directions are different and hence it will affect dendrite morphology and Zn metal deposition rate. Two terms D_{px} and D_{py} will be used, where D_{px} and D_{py} represent the diffusivity of Zn^{2+} in the protective layer in the x and y directions, respectively. We studied two cases: (i) for case 1, D_{px} is fixed at 1×10^{-11} m²/s and D_{py} increases, and (ii) for case 2, D_{py} is fixed at 1×10^{-11} m²/s and D_{py} increases the protrude size grows faster and almost becomes dendritic Zn, while the thickness of the planar anode surface grows slowly (**Figure 6(a)~(c)**). On the other hand, in case 2, when D_{px} increases, the planar anode surface grows faster and becomes thicker, while

the protrude size becomes smaller and does not turn into dendritic Zn (Figure 6(d)~(f)). To reveal the underlying mechanism of this phenomenon, we plot the Zn²⁺ flux for both cases using arrow graphs. In case 1, the flux is nonuniform at the Zn surface (Figure 6(g)), i.e., the flux is higher around the protrude, and the direction of flux is not perpendicular to the Zn surface. It is demonstrated that higher Zn²⁺ diffusivity in the y-direction promotes dendrite growth, which is attributed to the 2D diffusion of Zn²⁺ towards the protrude. On the contrary, in case 2, the flux is uniform at each surface, and the direction of the flux is perpendicular to the Zn surface (Figure 6(h)). It is clearly demonstrated that higher diffusivity of Zn^{2+} in the x-direction (perpendicular to Zn surface) hinders 2D lateral diffusion of Zn²⁺, which eventually leads to the inhibition of dendrite growth. It has been previously reported that 2D lateral diffusion of Zn²⁺ is responsible for the Zn dendrite formation and growth in Zn metal batteries. ^{21,47,53} Our simulation results thus agree well with prior experimental results. For comparison, the Zn²⁺ diffusivity is plotted versus the electrode thickness gain (Figure 6(i)) and dendrite tip height (Figure 6(j)). This comparison clearly indicates that electrode thickness increases with diffusivity for both cases (Figure 6(i)), but the growth rate is higher in case 2 (red curve), which is attributed to the higher Zn²⁺ flux (**Figure 6(h)**) in the protective layer. Meanwhile, the final height of the dendrite tip increases with diffusivity for case 1 (black curve) but decreases for case 2 (red curve) (Figure 6(i)), which is attributed to the 2D diffusion of Zn²⁺. Our simulation results thus indicate that enhancing the horizontal diffusivity of Zn^{2+} (D_{px}) via selecting/designing a proper protective layer can potentially inhibit the Zn dendrite growth and promote the Zn deposition rate in Zn metal batteries. The electric field and Zn²⁺ concentration for both cases are shown in **Figure S3**.

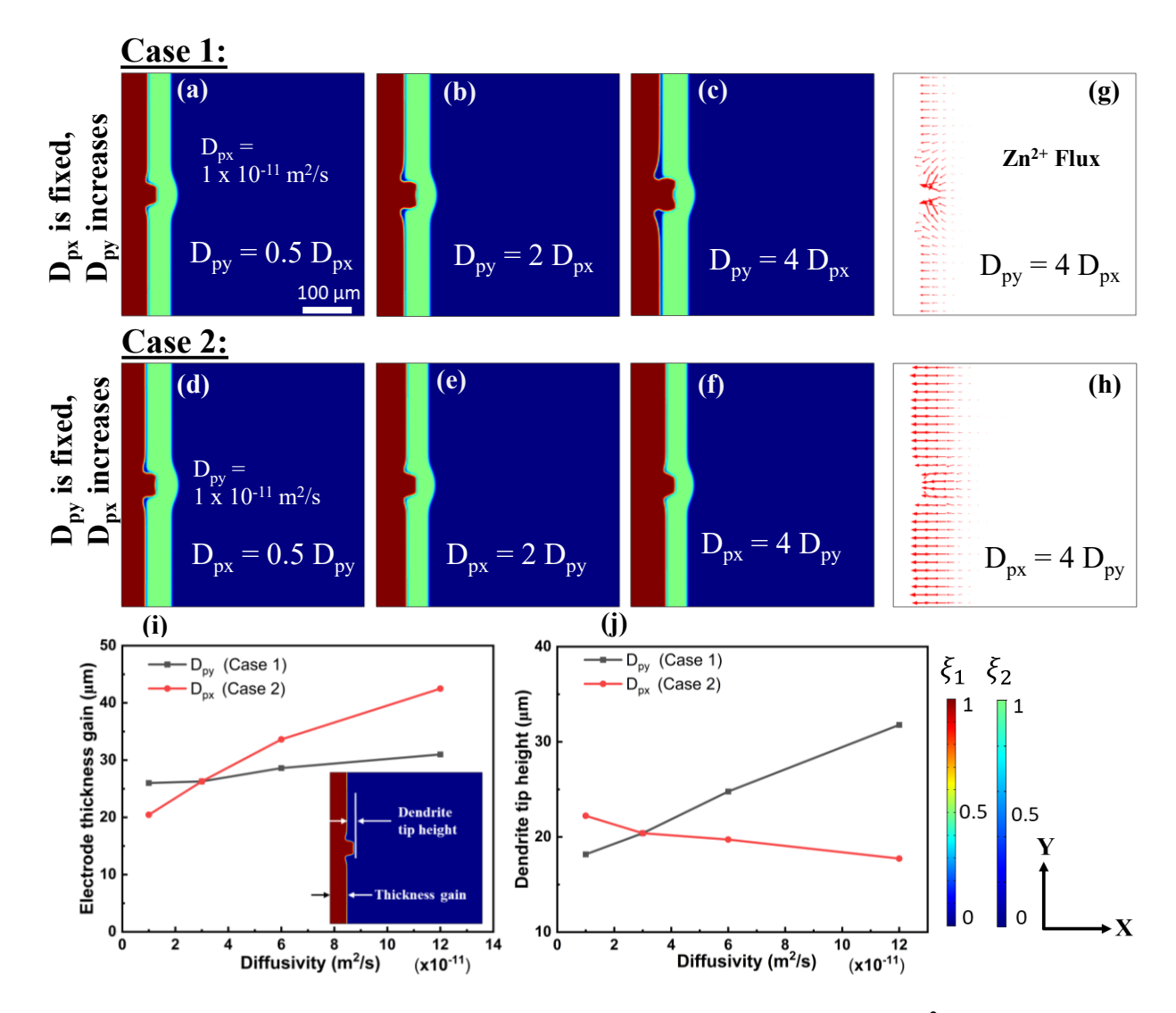


Figure 6. Simulation results showing the effect of anisotropic diffusion of Zn^{2+} in the protective layer on Zn metal growth (t = 300 s). (**a-c**) Final morphologies of Zn metal and protective layer when D_{px} is fixed and D_{py} increases. (**d-f**) Final morphologies of Zn metal and protective layer when D_{py} is fixed and D_{px} increases. (**g**) Zn^{2+} flux for case 1 when $D_{py} = 4D_{px}$. (**h**) Zn^{2+} flux for case 2 when $D_{px} = 4D_{py}$. (**i**) 1-D plot of electrode thickness gain versus diffusivity for both cases. (**j**) 1-D plot of dendrite tip height versus diffusivity for both cases. The scale bar in (**a**) applies to all figures (**a-h**).

In this study, we did not consider the mechanical strain effect of the protective layer. It is likely that dendrites may penetrate through the protective layer during deposition, due to the induced stress cracks may be formed in the protective layer, and delamination may happen. These will further influence the Zn deposition process. In our future studies, we will further develop our model to incorporate the elastic energy in the total free energy of the system and explore its effect on the Zn deposition.

4. Conclusion

In summary, we developed a phase-field model to study the effect of a highly Zn^{2+} diffusive protective layer on the suppression of Zn dendrite growth. Our model considers for the first time the dynamic interactions between the protective layer displacement and the Zn metal deposition. In the absence of the protective layer, the bare Zn metal grows into large dendritic structures due to a large electric field and concentration gradient segregated at the dendrite tip. However, when the protective layer is introduced on the top of the Zn anode, the dendrite growth is significantly inhibited. This is because the protective layer enables the homogenous distribution of Zn^{2+} and reduces the Zn^{2+} concentration gradient and electric field segregation. In addition, by increasing the diffusivity (isotropic) of Zn^{2+} in the protective layer, the growth rate of Zn metal increases, while the size of the protrudes remains almost the same. Finally, it is realized that higher diffusivity of Zn^{2+} in the x-direction homogenizes the Zn^{2+} flux by preventing 2D diffusion, resulting in smooth and dendrite-free deposition of Zn metal.

ASSOCIATED CONTENT

Supporting Information

A detailed description of the derivation of the driving force; boundary conditions; the simulation

results for the Zn²⁺ concentration and electric field for both isotropic and anisotropic diffusion

cases; and the thickness effect of the protective layer.

DECLARATION OF INTEREST

The authors declare no competing financial interest.

AUTHOR INFORMATION

Corresponding Author

Ye Cao – Department of Materials Science and Engineering, University of Texas at Arlington,

Texas 76019, United States.

Email: ye.cao@uta.edu

Authors

Bharat Pant – Department of Materials Science and Engineering, University of Texas at

Arlington, Texas 76019, United States

Yao Ren – Department of Materials Science and Engineering, University of Texas at Arlington,

Texas 76019, United States

Author Contributions

Y.C. initiated and supervised the project. Y.R. helped develop the phase-field model and provided

feedback on every step of the research. B.P. performed the phase-field simulations and wrote the

manuscript. All the authors have approved the final version of the manuscript.

ACKNOWLEDGMENTS

B.P. and Y.C. acknowledge the financial support from the National Science Foundation (NSF)

(Award No. 2038083) for doing this research.

23

References

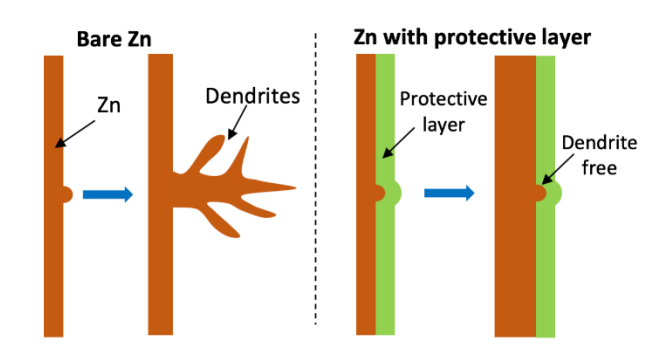
- Xie, S., Li, Y. & Dong, L. Stable anode-free zinc-ion batteries enabled by alloy network-modulated zinc deposition interface. *Journal of Energy Chemistry* **76**, 32-40 (2023). https://doi.org/https://doi.org/10.1016/j.jechem.2022.08.040
- Shi, X. et al. Homogeneous Deposition of Zinc on Three-Dimensional Porous Copper Foam as a Superior Zinc Metal Anode. ACS Sustainable Chemistry & Engineering 7, 17737-17746 (2019). https://doi.org/10.1021/acssuschemeng.9b04085
- Liu, S. *et al.* Regulating Li deposition by constructing homogeneous LiF protective layer for high-performance Li metal anode. *Chemical Engineering Journal* **427**, 131625 (2022). https://doi.org/https://doi.org/10.1016/j.cej.2021.131625
- Zhang, L. *et al.* Eliminating Dendrites and Side Reactions via a Multifunctional ZnSe Protective Layer toward Advanced Aqueous Zn Metal Batteries. *Advanced Functional Materials* **31**, 2100186 (2021). https://doi.org/10.1002/adfm.202100186
- Liu, S. et al. From room temperature to harsh temperature applications: Fundamentals and perspectives on electrolytes in zinc metal batteries. *Science Advances* 8, eabn5097 https://doi.org/10.1126/sciadv.abn5097
- Hao, J. et al. Designing Dendrite-Free Zinc Anodes for Advanced Aqueous Zinc Batteries. Advanced Functional Materials 30, 2001263 (2020). https://doi.org/https://doi.org/10.1002/adfm.202001263
- Wang, T. *et al.* Regulating Dendrite-Free Zinc Deposition by Red Phosphorous-Derived Artificial Protective Layer for Zinc Metal Batteries. *Advanced Science* **9**, 2200155 (2022). https://doi.org/https://doi.org/10.1002/advs.202200155
- Xie, F. et al. Mechanism for Zincophilic Sites on Zinc-Metal Anode Hosts in Aqueous Batteries. Advanced Energy Materials 11, 2003419 (2021). https://doi.org/https://doi.org/10.1002/aenm.202003419
- 9 Mu, Y. *et al.* Highly stable and durable Zn-metal anode coated by bi-functional protective layer suppressing uncontrollable dendrites growth and corrosion. *Chemical Engineering Journal* **430**, 132839 (2022). https://doi.org/https://doi.org/10.1016/j.cej.2021.132839
- Han, D. *et al.* A Corrosion-Resistant and Dendrite-Free Zinc Metal Anode in Aqueous Systems. *Small* **16**, 2001736 (2020). https://doi.org/https://doi.org/10.1002/smll.202001736
- Hong, L. *et al.* Toward Hydrogen-Free and Dendrite-Free Aqueous Zinc Batteries: Formation of Zincophilic Protective Layer on Zn Anodes. *Advanced Science* **9**, 2104866 (2022). https://doi.org/https://doi.org/10.1002/advs.202104866
- Liu, S. et al. Monolithic Phosphate Interphase for Highly Reversible and Stable Zn Metal Anode. Angewandte Chemie International Edition 62, e202215600 (2023). https://doi.org/https://doi.org/10.1002/anie.202215600
- Liu, M. et al. Artificial Solid-Electrolyte Interface Facilitating Dendrite-Free Zinc Metal Anodes via Nanowetting Effect. ACS Applied Materials & Interfaces 11, 32046-32051 (2019). https://doi.org/10.1021/acsami.9b11243
- Hu, K. *et al.* Stabilizing zinc metal anodes by artificial solid electrolyte interphase through a surface ion-exchanging strategy. *Chemical Engineering Journal* **396**, 125363 (2020). https://doi.org/https://doi.org/10.1016/j.cej.2020.125363
- Wang, F. *et al.* Highly reversible zinc metal anode for aqueous batteries. *Nature Materials* **17**, 543-549 (2018). https://doi.org/10.1038/s41563-018-0063-z

- Wang, S. *et al.* Low-Concentration Redox-Electrolytes for High-Rate and Long-Life Zinc Metal Batteries. *Small* **n/a**, 2207664 (2023). https://doi.org/https://doi.org/10.1002/smll.202207664
- Huang, C. *et al.* Self-Healing SeO2 Additives Enable Zinc Metal Reversibility in Aqueous ZnSO4 Electrolytes. *Advanced Functional Materials* **32**, 2112091 (2022). https://doi.org/https://doi.org/10.1002/adfm.202112091
- Liu, D. *et al.* Self-Healing Solid Polymer Electrolyte with High Ion Conductivity and Super Stretchability for All-Solid Zinc-Ion Batteries. *ACS Applied Materials & Interfaces* **13**, 36320-36329 (2021). https://doi.org/10.1021/acsami.1c09200
- 19 Chen, Z. *et al.* Grafted MXene/polymer electrolyte for high performance solid zinc batteries with enhanced shelf life at low/high temperatures. *Energy & Environmental Science* **14**, 3492-3501 (2021). https://doi.org/10.1039/D1EE00409C
- 20 Ma, L. *et al.* Liquid-Free All-Solid-State Zinc Batteries and Encapsulation-Free Flexible Batteries Enabled by In Situ Constructed Polymer Electrolyte. *Angewandte Chemie International Edition* **59**, 23836-23844 (2020). https://doi.org/https://doi.org/https://doi.org/10.1002/anie.202011788
- Zhang, Y. *et al.* Dendrites-Free Zn Metal Anodes Enabled by an Artificial Protective Layer Filled with 2D Anionic Nanosheets. *Small Methods* **5**, 2100650 (2021). https://doi.org/https://doi.org/10.1002/smtd.202100650
- Yang, Z. *et al.* Revealing the Two-Dimensional Surface Diffusion Mechanism for Zinc Dendrite Formation on Zinc Anode. *Small* **18**, 2104148 (2022). https://doi.org/https://doi.org/10.1002/smll.202104148
- Zhao, Z. *et al.* Long-life and deeply rechargeable aqueous Zn anodes enabled by a multifunctional brightener-inspired interphase. *Energy & Environmental Science* **12**, 1938-1949 (2019). https://doi.org/10.1039/C9EE00596J
- Yang, Y. *et al.* Redistributing Zn-ion flux by interlayer ion channels in Mg-Al layered double hydroxide-based artificial solid electrolyte interface for ultra-stable and dendrite-free Zn metal anodes. *Energy Storage Materials* **41**, 230-239 (2021). https://doi.org/https://doi.org/10.1016/j.ensm.2021.06.002
- Zhou, B. *et al.* A multifunctional protective layer with biomimetic ionic channel suppressing dendrite and side reactions on zinc metal anodes. *Journal of Colloid and Interface Science* **613**, 136-145 (2022). https://doi.org/https://doi.org/10.1016/j.jcis.2022.01.027
- Yang, Q. et al. Dendrites in Zn-Based Batteries. Advanced Materials **32**, 2001854 (2020). https://doi.org/https://doi.org/10.1002/adma.202001854
- Wang, T. *et al.* Spirally Grown Zinc-Cobalt Alloy Layer Enables Highly Reversible Zinc Metal Anodes. *Advanced Functional Materials* **n/a**, 2306101 (2023). https://doi.org/https://doi.org/10.1002/adfm.202306101
- 28 Li, D. *et al.* Self-assembled multilayers direct a buffer interphase for long-life aqueous zinc-ion batteries. *Energy & Environmental Science* **16**, 3381-3390 (2023). https://doi.org/10.1039/D3EE01098H
- Zhong, Y. *et al.* Triple-function Hydrated Eutectic Electrolyte for Enhanced Aqueous Zinc Batteries. *Angewandte Chemie International Edition* **62**, e202310577 (2023). https://doi.org/https://doi.org/10.1002/anie.202310577
- Guyer, J. E., Boettinger, W. J., Warren, J. A. & McFadden, G. B. Phase field modeling of electrochemistry. I. Equilibrium. *Physical Review E* **69**, 021603 (2004). https://doi.org/10.1103/PhysRevE.69.021603
- Guyer, J. E., Boettinger, W. J., Warren, J. A. & McFadden, G. B. Phase field modeling of electrochemistry. II. Kinetics. *Physical Review E* **69**, 021604 (2004). https://doi.org/10.1103/PhysRevE.69.021604

- Liang, L. *et al.* Nonlinear phase-field model for electrode-electrolyte interface evolution. *Physical Review E* **86**, 051609 (2012). https://doi.org/10.1103/PhysRevE.86.051609
- Liang, L. & Chen, L.-Q. Nonlinear phase field model for electrodeposition in electrochemical systems. *Applied Physics Letters* **105**, 263903 (2014). https://doi.org/10.1063/1.4905341
- Chen, L. *et al.* Modulation of dendritic patterns during electrodeposition: A nonlinear phase-field model. *Journal of Power Sources* **300**, 376-385 (2015). https://doi.org/https://doi.org/10.1016/j.jpowsour.2015.09.055
- Hong, Z., Ahmad, Z. & Viswanathan, V. Design Principles for Dendrite Suppression with Porous Polymer/Aqueous Solution Hybrid Electrolyte for Zn Metal Anodes. *ACS Energy Letters* **5**, 2466-2474 (2020). https://doi.org/10.1021/acsenergylett.0c01235
- Ren, Y., Zhou, Y. & Cao, Y. Inhibit of Lithium Dendrite Growth in Solid Composite Electrolyte by Phase-Field Modeling. *The Journal of Physical Chemistry C* **124**, 12195-12204 (2020). https://doi.org/10.1021/acs.jpcc.0c01116
- Ren, Y., Zhang, K., Zhou, Y. & Cao, Y. Phase-Field Simulation and Machine Learning Study of the Effects of Elastic and Plastic Properties of Electrodes and Solid Polymer Electrolytes on the Suppression of Li Dendrite Growth. *ACS Applied Materials & Interfaces* **14**, 30658-30671 (2022). https://doi.org/10.1021/acsami.2c03000
- Tantratian, K., Yan, H., Ellwood, K., Harrison, E. T. & Chen, L. Unraveling the Li Penetration Mechanism in Polycrystalline Solid Electrolytes. *Advanced Energy Materials* **11**, 2003417 (2021). https://doi.org/https://doi.org/10.1002/aenm.202003417
- Tian, H.-K., Liu, Z., Ji, Y., Chen, L.-Q. & Qi, Y. Interfacial Electronic Properties Dictate Li Dendrite Growth in Solid Electrolytes. *Chemistry of Materials* **31**, 7351-7359 (2019). https://doi.org/10.1021/acs.chemmater.9b01967
- Chen, C.-H. & Pao, C.-W. Phase-field study of dendritic morphology in lithium metal batteries. *Journal of Power Sources* **484**, 229203 (2021).

 https://doi.org/https://doi.org/10.1016/j.jpowsour.2020.229203
- Yan, H. H., Bie, Y. H., Cui, X. Y., Xiong, G. P. & Chen, L. A computational investigation of thermal effect on lithium dendrite growth. *Energy Conversion and Management* **161**, 193-204 (2018). https://doi.org/https://doi.org/10.1016/j.enconman.2018.02.002
- Hong, Z. & Viswanathan, V. Prospect of Thermal Shock Induced Healing of Lithium Dendrite. *ACS Energy Letters* **4**, 1012-1019 (2019). https://doi.org/10.1021/acsenergylett.9b00433
- Cao, D. *et al.* Nondestructively Visualizing and Understanding the Mechano-Electro-chemical Origins of "Soft Short" and "Creeping" in All-Solid-State Batteries. *Advanced Functional Materials* **n/a**, 2307998 (2023). https://doi.org/https://doi.org/10.1002/adfm.202307998
- Yurkiv, V. et al. Understanding Zn Electrodeposits Morphology in Secondary Batteries Using Phase-Field Model. *Journal of The Electrochemical Society* **167**, 060503 (2020). https://doi.org/10.1149/1945-7111/ab7e91
- 45 Yang, C. *et al.* Explicit Dynamics of Diffuse Interface in Phase-Field Model. *Advanced Theory and Simulations* **4**, 2000162 (2021). https://doi.org/https://doi.org/10.1002/adts.202000162
- Cogswell, D. A. Quantitative phase-field modeling of dendritic electrodeposition. *Physical Review E* **92**, 011301 (2015). https://doi.org/10.1103/PhysRevE.92.011301
- Xie, D. *et al.* Polymeric Molecular Design Towards Horizontal Zn Electrodeposits at Constrained 2D Zn2+ Diffusion: Dendrite-Free Zn Anode for Long-Life and High-Rate Aqueous Zinc Metal Battery. *Advanced Functional Materials* **32**, 2204066 (2022). https://doi.org/https://doi.org/10.1002/adfm.202204066
- Zhang, Y. *et al.* Nonionic Surfactant-Assisted In Situ Generation of Stable Passivation Protective Layer for Highly Stable Aqueous Zn Metal Anodes. *Nano Letters* **22**, 8574-8583 (2022). https://doi.org/10.1021/acs.nanolett.2c03114

- Zhou, S. *et al.* Anti-Corrosive and Zn-Ion-Regulating Composite Interlayer Enabling Long-Life Zn Metal Anodes. *Advanced Functional Materials* **31**, 2104361 (2021). https://doi.org/https://doi.org/10.1002/adfm.202104361
- Wang, K. *et al.* Dendrite growth in the recharging process of zinc–air batteries. *Journal of Materials Chemistry A* **3**, 22648-22655 (2015). https://doi.org/10.1039/C5TA06366C
- Yang, Y. *et al.* Synergistic Manipulation of Zn2+ Ion Flux and Desolvation Effect Enabled by Anodic Growth of a 3D ZnF2 Matrix for Long-Lifespan and Dendrite-Free Zn Metal Anodes. *Advanced Materials* **33**, 2007388 (2021). https://doi.org/https://doi.org/10.1002/adma.202007388
- Pan, L., He, H., Liu, Z. & Hu, P. Redistributing zinc-ion flux by constructing a hybrid conductor interface for dendrite-free zinc anode. *Journal of Power Sources* **551**, 232173 (2022). https://doi.org/https://doi.org/10.1016/j.jpowsour.2022.232173
- Xie, S. et al. Stable Zinc Anodes Enabled by Zincophilic Cu Nanowire Networks. *Nano-Micro Letters* **14**, 39 (2021). https://doi.org/10.1007/s40820-021-00783-4



For Table of Contents Only